

Gentle Driving of Piles (GDP) at a sandy site combining axial and torsional vibrations Part I - installation tests

Tsetas, Athanasios; Tsouvalas, Apostolos ; Sánchez Gómez, Sergio ; Pisano, Federico; Kementzetzidis, Evangelos; Molenkamp, Timo; Elkadi, Ahmed S.K. ; Metrikine, Andrei

DOI

[10.1016/j.oceaneng.2022.113453](https://doi.org/10.1016/j.oceaneng.2022.113453)

Publication date

2023

Document Version

Final published version

Published in

Ocean Engineering

Citation (APA)

Tsetas, A., Tsouvalas, A., Sánchez Gómez, S., Pisano, F., Kementzetzidis, E., Molenkamp, T., Elkadi, A. S. K., & Metrikine, A. (2023). Gentle Driving of Piles (GDP) at a sandy site combining axial and torsional vibrations: Part I - installation tests. *Ocean Engineering*, 270, Article 113453. <https://doi.org/10.1016/j.oceaneng.2022.113453>

Important note

To cite this publication, please use the final published version (if applicable).
Please check the document version above.

Copyright

Other than for strictly personal use, it is not permitted to download, forward or distribute the text or part of it, without the consent of the author(s) and/or copyright holder(s), unless the work is under an open content license such as Creative Commons.

Takedown policy

Please contact us and provide details if you believe this document breaches copyrights.
We will remove access to the work immediately and investigate your claim.



Gentle Driving of Piles (GDP) at a sandy site combining axial and torsional vibrations: Part I - installation tests

Athanasios Tsetas^a, Apostolos Tsouvalas^a, Sergio S. Gómez^a, Federico Pisanò^{a,*}, Evangelos Kementzetzidis^a, Timo Molenkamp^a, Ahmed S.K. Elkadi^b, Andrei V. Metrikine^a

^a Faculty of Civil Engineering and Geosciences, Delft University of Technology, Stevinweg 1, Delft, 2628 CN, The Netherlands

^b Deltares, Boussinesqweg 1, Delft, 2629 HV, The Netherlands

ARTICLE INFO

Keywords:
Pile driving
Monopiles
Soil/structure interaction
Dynamics

ABSTRACT

Gentle Driving of Piles (GDP) is a new technology for the vibratory installation of tubular (mono)piles. Its founding principle is that both efficient installation and low noise emission can be achieved by applying to the pile a combination of axial and torsional vibrations. Preliminary development and demonstration of the proposed technology are the main objectives of the GDP research programme. To this end, onshore medium-scale tests in sand have been performed on piles installed using both impact and vibratory driving methods (including GDP). After presenting the development of a purpose-built GDP driving device and the geotechnical characterisation of the site, this paper covers the execution of GDP installation tests. Focus is on the installation performance of GDP-driven piles, which is discussed with the aid of structural and ground monitoring data. The comparison between piling data associated with GDP and standard axial vibro-driving points out the potential of the proposed installation technology, particularly with regard to the beneficial effect of the torsional vibration component. The findings of this study encourage further development of the GDP method and its future extension to offshore full-scale conditions.

1. Introduction

Ever more countries worldwide are working to shift their energy mix towards renewables. The Netherlands, country of origin of this study, is actively contributing to the European decarbonisation agenda (European Commission, 2020) by promoting the exploitation of renewable energy sources, both onshore and offshore (Minister of Economic Affairs and Climate Policy, 2020). In this regard, offshore wind energy will continue to play an increasingly relevant role as an abundant, cost-effective resource (Ramírez et al., 2021), on the condition that the pace of its technological development is further expedited. Presently, 15%–24% of the investment for the construction of an offshore wind farm relates to the design, production, and installation of substructures (Stehly and Beiter, 2020). Continual improvement of engineering methodologies in this area is therefore key to achieving further cost reduction (Byrne et al., 2019; Page et al., 2019; Wu et al., 2019).

As reported in the latest EWEA report (Ramírez et al., 2021), over 80% of the existing offshore wind turbines (OWTs) in European wind farms are founded on so-called monopile foundations, which are most commonly installed by means of impact hammering. The

impact technology is to date very well established in the offshore industry (Kallehave et al., 2015). However, impact installation in certain soil conditions (e.g., dense sands) may be slower than desired (Rodger and Littlejohn, 1980; Achmus et al., 2020), which causes increased installation costs and, possibly, higher pile damage under many hammer blows (Mosher, 1987; Meijers et al., 2018). Moreover, the underwater noise emitted during pile installation is known to be harmful to marine life, and has motivated over the years the enforcement of strict regulations to limit its negative environmental effects (Tsouvalas, 2020). Such regulations include the adoption of costly soundproofing measures (e.g., bubble curtains, isolation casings, and cofferdams) (Koschinski and Lüdemann, 2013; Tsouvalas and Metrikine, 2016a).

An interesting alternative to impact piling is provided by vibratory technologies, which can achieve quiet(er)/fast pile installation through the application of low-amplitude axial vibrations. The input excitation is induced through the harmonic rotation of eccentric masses, usually at a frequency no larger than 40 Hz. Vibratory pile hammers (or simply ‘vibro-hammers’) have been manufactured and studied since the 1940s (Rodger and Littlejohn, 1980), and their benefits in terms of driving performance and noise emission are known since then (Barkan, 1967; Mosher, 1987, 1990; Tsouvalas and Metrikine, 2016b). The use

* Corresponding author.

E-mail address: f.pisano@tudelft.nl (F. Pisanò).

<https://doi.org/10.1016/j.oceaneng.2022.113453>

Received 26 April 2022; Received in revised form 25 October 2022; Accepted 4 December 2022

Available online 12 January 2023

0029-8018/© 2023 The Author(s). Published by Elsevier Ltd. This is an open access article under the CC BY license (<http://creativecommons.org/licenses/by/4.0/>).

List of acronyms and symbols

ATP	Auxiliary test pile
B1,B2	Soil batches from borehole material
CPTu	Cone penetration testing with pore water pressure measurement
CSL	Crosshole sonic logging
CV-25	Axial vibratory device
DL	Driving logging system
DSI	Detailed site investigation
FBG	Fiber Bragg grating sensors
GDP ₁ , GDP ₂	Piles installed via GDP driving
GDP ₀₁ , GDP ₀₂	Auxiliary piles installed via GDP driving
GDP	Gentle Driving of Piles
HPT-MPT	Hydro-profiling tests with mini pump tests
HPU	Hydraulic power unit
IH	Pile installed via impact hammering
MEMS	Micro-electro-mechanical systems
MTP	Main test pile
NAP	<i>Normaal Amsterdams Peil</i>
PM	Potentiometer
PPT	Pore water pressure transducers
PSI	Preliminary site investigation
SAAV	Shape acceleration array
SBTn	Normalized soil behaviour type
SCPTu	Seismic cone penetration testing with pore water pressure measurement
SPC	Soil pressure cell
STFT	Short-time Fourier transform
VH	Pile installed via axial vibratory driving
a_r	Radial pile acceleration
a_z	Axial pile acceleration
a_θ	Circumferential pile acceleration
C_c	Coefficient of curvature (from PSD curves)
C_u	Coefficient of uniformity (from PSD curves)
D	Pile diameter
D_r	Relative density
D_{50}	Size of particle at 50% point on particle size distribution curve
d	Soil particle diameter
E	Energy
e_{max}	Soil's maximum void ratio
e_{min}	Soil's minimum void ratio
F_a	Axial force
F_r	Normalised friction ratio
f	Frequency
G_s	Specific gravity
h	Pile wall thickness
k_h	Horizontal hydraulic conductivity
L	Pile length

L_e	Embedded pile length
M_t	Torsional moment
$m_a e_a$	Eccentric moment of axial excitation
$m_t e_t$	Eccentric moment of torsional excitation
P	Power
p_w	Pore water pressure
Q_{in}	Normalised cone resistance
\bar{q}_c	Average cone resistance
q_c	Cone resistance
R_t	Distance between pile centre and eccentric masses for torsion
t	Time
\bar{u}	Average penetration rate
\dot{u}	Penetration rate
u	Penetration
V_p	Compression wave velocity
V_s	Shear wave velocity
W	Cumulative percentage (%) of soil mass retained on any sieve
z	Soil depth coordinate (under ground surface)
Δp_w	Variation of pore water pressure
$\Delta \sigma_r$	Variation of radial soil stress
σ_r	Radial soil stress
Ω_a	Frequency of axial excitation
Ω_t	Frequency of torsional excitation

of piling loads lower than in impact driving can effectively reduce both damage and radial expansion of the pile during driving — the latter (Poisson effect) is a major culprit for noise emission and larger soil resistance to driving (De Nicola and Randolph, 1993). Despite its obvious benefits, vibratory driving is not yet widely adopted for offshore piling. Its use is hindered by a number of factors, including the incompleteness (and inconclusiveness) of available field observations. Major knowledge gaps are also associated with soil's dynamic behaviour during

vibro-driving (Mazza and Holeyman, 2019) and the effects of vibro-installation on the operational performance of the pile (Anusic et al., 2019; Tsetas et al., 2020; Achmus et al., 2020).

To boost the improvement of vibro-piling methods, a new technology – Gentle Driving of Piles (GDP) – has been recently proposed in the Netherlands as core of a joint industry project led by the Delft University of Technology (TU Delft) (Metrikine et al., 2020). GDP targets enhanced piling performance and reduced noise emissions through the simultaneous application of low-frequency/axial and high-frequency/torsional vibrations. This thread of research was originally inspired by observing that torsional vibrations do not induce radial pile expansion during driving, which was foreseen to play in favour of both driving and acoustic performances. A preliminary demonstration of the proposed technology was pursued by performing medium-scale field tests on identical test piles installed using impact and vibratory driving methods, including GDP. The tests were performed in sandy soil at the Port of Rotterdam and comprised two distinct stages, the first to investigate the driving performance, and the second to explore installation effects in the response of the test piles to repeated lateral loading — see also the companion paper by Kementzetzidis et al. (2023). The GDP field campaign adds to the research carried out within other major programmes on monopile foundations, such as PISA (Byrne et al., 2019) and PICASO (Byrne et al., 2020) in the UK, REDWIN (Skau et al., 2018) and WAS-XL (Page et al., 2020) in Norway, Vibro (Herwig and Gattermann, 2015; Achmus et al., 2020) in Germany, and DISSTINCT (Versteijlen et al., 2017), MIDAS (Pisanò et al., 2022) and BLUE Piling (IQIP, 2020) in the Netherlands.

The GDP project was initiated to achieve a preliminary demonstration of the proposed pile driving method at medium scale — particularly, with respect to the inclusion of a high-frequency torsional vibration component (almost three times higher its axial counterpart). In what follows, the installation performance of two GDP-driven piles is described in detail with the aid of selected field measurements, and in comparison to other piling data associated with standard axial vibro-driving. Although the GDP project was originally motivated by offshore



Fig. 1. The GDP shaker: (a) view at the manufacturing site; (b) shaker connected to a test pile via a bolted flange connection.

wind developments, this paper aims to attract the interest of the piling community, and foster further studies for an even broader range of applications and geotechnical conditions.

2. The GDP shaker

The design of the GDP shaker built on the idea of installing monopiles by combining low-frequency/axial and high-frequency/torsional motions. The effectiveness of such a pile driving approach was envisioned in light of the following considerations:

- (i) high-frequency torsional motion is expected to reduce the axial frictional resistance along the pile shaft. Since torsional vibration mobilises soil shear resistance in the circumferential direction, less frictional resources are left to oppose axial pile penetration (Georgiadis and Saflekou, 1990; Holeyman, 2002);
- (ii) as a consequence of point (i), the axial vibratory load that is necessary to drive the pile can be reduced, so that the amplitude of the generated stress waves will decrease in comparison to the case of purely axial vibro-driving. Therefore, the amplitude of the radial pile motion (Poisson effect) will also decrease, as a result of the so-called ring frequency effect (Tsouvalas and Metrikine, 2013; Tsetas et al., 2021);
- (iii) the mentioned decrease in radial pile expansion during installation is believed to be beneficial for two reasons. First, it is expected to enable faster penetration, due to lower soil confinement; secondly, less radial expansion of the pile results in reduced underwater noise emissions.

It is worth recalling that, under axisymmetric loading conditions (e.g., in the presence of a torque), the circumferential motion of an elastic cylindrical structure (pile) is uncoupled from its axial and radial components (Forsberg, 1969). Therefore, a pile subjected to torsional vibrations can only transmit shear (SH) waves to the surrounding media (Kausel, 2006). Such shear waves cannot propagate in seawater (Jensen et al., 2011), nor do they contribute to underwater noise.

Importantly, the preference for torsional vibrations at high frequency relates to the short wavelengths that are accordingly transmitted to the soil, which decay in amplitude within a short distance from the pile. Therefore, the torsional mobilisation of the soil resistance (also reduced by pore pressure build-up Holeyman, 2002) is expected to occur locally around the pile shaft, and likely with a lower impact on

the post-installation lateral response than in the case of low-frequency axial vibrations.

A novel GDP shaker was designed and purpose-built for the execution of GDP-driving tests (Fig. 1). As shown in Fig. 2, the shaker is formed by three gear trains directly connected to masses that can counter-rotate with a given (constant) eccentricity. Such masses are accommodated within exciter blocks, which are in turn bolted to a support structure. In its first design, the GDP shaker operated by means of hydraulic motors and was connected to each test pile via a bolted flange connection, which was a preliminary solution adopted for the GDP experimental campaign (see Fig. 1).

Similarly to conventional vibratory hammers, the eccentric masses in the GDP shaker are set to counter-rotate in order to generate a dynamic load along a selected direction. In the case of the GDP shaker, the exciter block at the top of the support structure can generate a harmonic load $F_a(t)$ along the pile axis with frequency Ω_a . To induce torsional and axial vibrations of different amplitude and frequency, a separate set of exciter blocks was needed. To this end, two additional exciter blocks were mechanically connected through a shaft with the twofold goal of (i) assembling all units into a single substructure and (ii) positioning them properly. Furthermore, vibratory loads were generated based on a control system that ensured synchronisation, so as to obtain the application of a torque $M_t(t)$ of frequency Ω_t at the top of the pile (Fig. 2). Overall, the GDP shaker can apply to the pile head load combinations of the following type:

$$F_a(t) = m_a e_a \Omega_a^2 \sin(\Omega_a t) \quad (1)$$

$$M_t(t) = R_t m_t e_t \Omega_t^2 \sin(\Omega_t t) \quad (2)$$

where $m_a \cdot e_a$ and $m_t \cdot e_t$ denote, respectively, the axial and torsional eccentric moments¹ associated with the eccentric masses in both exciter blocks. The distance between the centre of the pile cross-section and the torsional eccentric masses is denoted by R_t (see Fig. 2). According to Eqs. (1) and (2), the resulting load amplitudes are mainly governed by the frequency as the eccentric moments ($m_a \cdot e_a$ and $m_t \cdot e_t$) and the radius (R_t) are fixed.

Fig. 3 illustrates the axial and torsional inputs generated based on the counter-rotation of the respective eccentric masses, along with their representation as part of a pile-soil interaction model. The axial load

¹ Although not rigorously moments, $m_a \cdot e_a$ and $m_t \cdot e_t$ are usually referred to as such within the vibro-driving community.

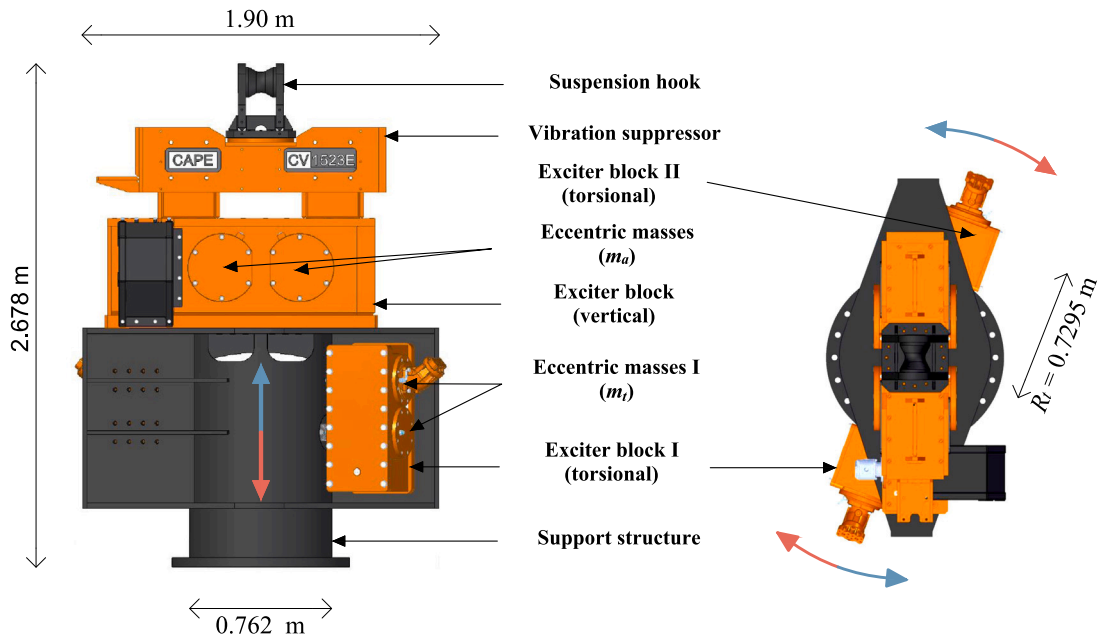


Fig. 2. Detailed design of the GDP shaker.

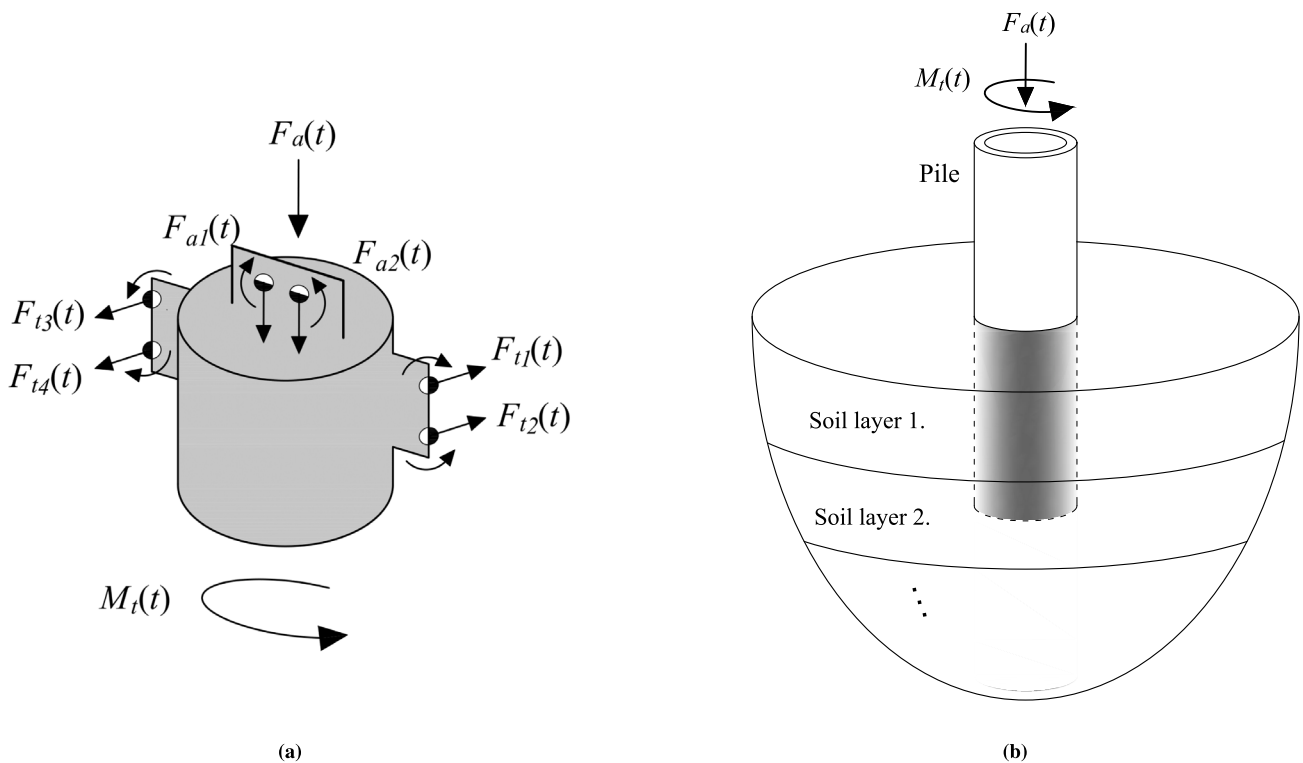


Fig. 3. (a) Generation of axial and torsional loads through the rotating eccentric masses in the GDP shaker; (b) sketch of a pile-soil interaction model in the presence of axial and torsional loads during GDP-driving.

corresponds with the force resultant of $F_{a1}(t)$ and $F_{a2}(t)$, whereas the torque is the net moment resultant of $F_{t1}(t)$, $F_{t2}(t)$, $F_{t3}(t)$, and $F_{t4}(t)$; it is remarked that the net force resultant of the latter set of forces is always equal to zero. Further details regarding GDP shaker specifications may be found in Gómez and Metrikine (2021).

The final design of the GDP shaker stemmed directly from the conceptual foundation of the GDP method, though with constraints imposed by practical limitations. In the installation tests described in the following, the axial vibration frequency of GDP was set to be

similar to the frequency adopted for a parallel axial vibro-driving test, so as to gain insight into the effect of the torsional vibrations. On the other hand, the GDP torsional frequency was maximised within the manufacturing constraints of the GDP shaker. In particular, the choice of the torsional frequency was driven by the need of maintaining comparable power capacity for the installation tests associated both with GDP and axial vibro-driving. The final design of the GDP shaker enabled the application of axial and torsional vibratory loads with frequencies up to 23 Hz and 80 Hz, respectively.

Table 1
Technical specifications of the GDP shaker and the axial vibro-hammer CV-25.

	GDP shaker		Axial vibro-hammer CV-25
	Axial shaker	Torsional shaker	Axial shaker
Total mass [kg]	5150		4100
Eccentric moment m_e [kg m]	15	4	25
Rotational speed [rpm]	1400	4800	1800
Operational power [kW]	72	188	263

The main technical specifications of the GDP shaker and the standard vibratory hammer (CV-25) used in the GDP campaign are summarised in Table 1.

3. Geotechnical site characterisation

The execution of field tests in onshore conditions is generally advantageous prior to full-scale offshore demonstration, in light of the better control of testing conditions that can be obtained by deploying equipment on land. The GDP experimental campaign was planned to achieve a preliminary proof of concept for the proposed pile driving technology. To this end, medium-scale onshore field tests in sandy soil were performed. Both geotechnical and logistical considerations led to the selection of the Maasvlakte II site at the Port of Rotterdam, which offers space and facilities for field tests and is presently supporting an increasing number of offshore-related demonstration projects. This part of the port comprises North Sea sand that was used to create a reclaimed/compacted site. The GDP field tests took place at the Maasvlakte II over a surface of $60 \times 60 \text{ m}^2$ in the so-called *area E*. Site location and access routes are shown in Fig. 4.

3.1. Site investigation

The geotechnical investigation of the test site was carried out between June and September 2019 in two phases of *preliminary* and *detailed* site investigation (PSI and DSI, respectively). First, the PSI was performed to identify suitable locations for installing the test piles, mostly in light of site homogeneity considerations. During the PSI, 25 cone penetration tests with pore water pressure measurements (CPTu) were performed down to a target depth of 10 m over a regular grid with a spacing of about 12.5 m. After reaching the target depth, dissipation tests were executed for the CPTu's at the four corners to measure the depth of the ground water table. Each dissipation test lasted for one hour, which was deemed sufficient for the achievement of hydraulic steady-state conditions. Based on these tests, the depth of the water table was estimated to range, at the time of the PSI, between 3.5 and 4.5 m depth below the ground surface (phreatic fluctuations are to be expected at the test site due to its proximity to open waters).

After selecting all pile locations based on the PSI, the DSI phase was carried out by performing additional tests around and at the centre of each pile location (see Fig. 5). Eight test piles were installed along with a larger reaction pile (RP). The latter would later serve the post-installation loading tests described in the companion paper (Kementzetzidis et al., 2023). The embedded length was 8 m for all piles, i.e., 2 m less than the target depth of the CPTu's. Four of the test piles, henceforth referred to as *Main Test Piles* (MTPs), were extensively instrumented and installed with a radial, centre-to-centre distance of 12 m from the RP. The other four piles, labelled as *Auxiliary Test Piles* (ATPs), were installed uninstrumented for preliminary testing purposes, at a distance of 16 m from the RP (Fig. 5). As detailed in the following, the four MTPs were installed using different driving methods, namely impact hammering (IH), axial vibro-driving (VH), and GDP — see Fig. 5. For the two standard driving methods, the Hydrohammer S-90 and the vibro-hammer CV-25 were used for the IH and VH piles, respectively.

The DSI programme included:

- four CPTu tests at the ATP locations (target depth: 10 m);



Fig. 4. GDP test site and its access routes — edited after (OpenStreetMap contributors, 2017).

- four Seismic CPTu (SCPTu) tests at the MTP locations (target depth: 10 m);
- four hydro-profiling tests with mini pump tests (HPT-MPT) around the MTPs (target depth: 15 m).
- borehole sampling around the MTPs. A total of eight boreholes (two per MTP) of 10 m depth and 15 cm diameter were dug and simultaneously sustained with hollow PVC tubes, which would then enable the execution of Cross-hole Sonic Logging (CSL) tests;
- three boreholes (15 cm diameter) around each MTP to host ground monitoring instrumentation, including Shape Acceleration Arrays (SAAVs), soil pressure cells (SPCs), and pore water pressure transducers (PPTs). As shown in Fig. 5, two pairs of SPC and PPT sensors were installed in two different boreholes to reach different target depths (6 m and 8 m).

Layout and locations of DSI tests and boreholes are shown on the right side of Fig. 5 for the case of the MTP GDP₁. Both PSI and DSI data confirmed the predominantly sandy nature of the soil deposit from the ground surface (NAP +5 m – *Normaal Amsterdams Peil*, i.e., *Amsterdam Ordnance Datum*) down to approximately 10 m below (NAP –5 m). The upper 5 m consist of the dredged material employed to create the Maasvlakte II site, which overlays a layer of sand and clayey/silty sand from the holocene Naaldwijk formation (Vos, 2015).

The whole SCPTu dataset is visualised in Fig. 6 after post-processing according to Robertson's soil classification framework (*SBTn charts*) (Robertson, 1990, 2009). Robertson's approach relies on the notion of *normalised soil behaviour type*, which is identified for any soil at hand based on the values of relevant dimensionless indices — namely, the normalised cone resistance (Q_{tn}) and the normalised friction ratio (F_r). In Fig. 6, all data points from the four soil profiles lie mostly in zone 6 (sand), with some excursions into zone 5 (sand-mixtures) and zone 7 (gravelly sand to sand). The cone penetration data from the four MTP locations indicate altogether reasonably consistent profiles of soil type/properties — see Figs. 7(a)-7(c).

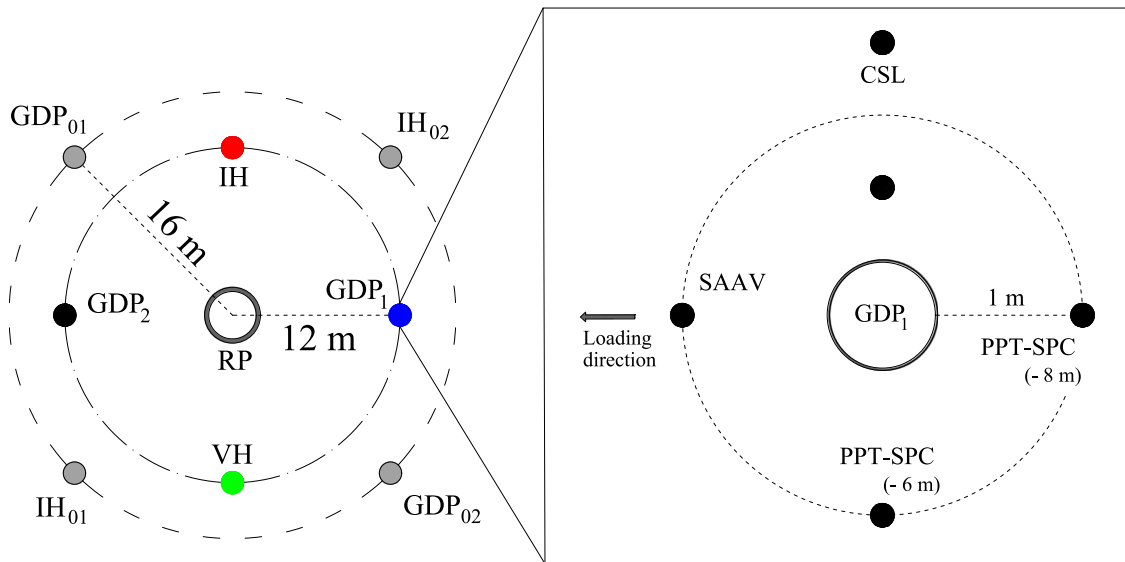


Fig. 5. Site layout (left — ATPs in grey) and soil monitoring around the MTPs (right). For better readability, the site layout on the left is shown with MTP diameters and distances from the central RP that are not to scale.

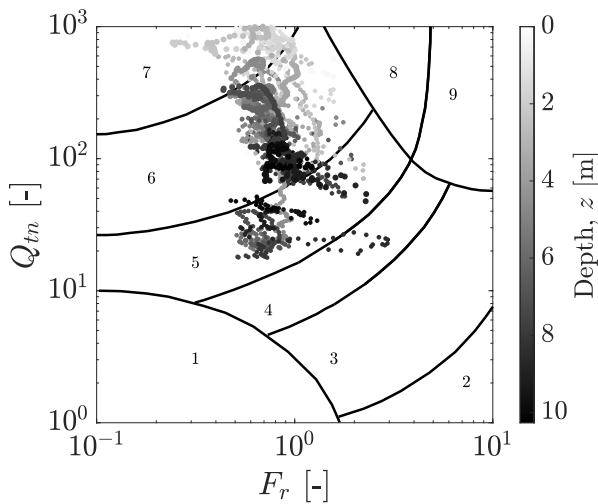


Fig. 6. Robertson's soil classification at the four MTP locations.

The profiles in Fig. 7 of (a) cone resistance (q_c), (b) shear wave velocity (V_s), and (c) relative density (D_r) (obtained following Jamiolkowski et al., 2003) suggest that the site comprises very dense sand ($D_r = 80 - 100\%$) in the upper 5 m, and medium-dense to dense sand ($D_r = 60 - 80\%$) in the 5 m below. An exception can be observed at the VH pile location (Fig. 7), where the SCPTu data show much lower cone resistance and relative density ($D_r < 40\%$) in the lower 5 m. Obviously, the effects of this site anomaly will require special attention when comparing the results of different pile tests.

The V_s profiles obtained from seismic measurements are largely consistent with the corresponding $q_c - D_r$ distributions, with V_s values mostly in the range from 200 to 300 m/s (and occasionally up to 350 m/s). The VH location exhibits the same aforementioned anomaly also in terms of V_s – note that a significant portion of the profile exhibits V_s values lower than 150 m/s.

Finally, Fig. 7(d) displays the hydraulic conductivity profiles (k_h , horizontal component) obtained next to the four MTPs. The k_h values shown in the figure lie mostly in the range of 10^{-4} – 10^{-3} m/s (average permeability of 4.45×10^{-4} m/s over the first 10 m), which is in line with expectations for the type of sandy soil found at the Maasvlakte II

Table 2

Index properties of Maasvlakte II sand (G_s – specific gravity; e_{max} – maximum void ratio; e_{min} – minimum void ratio; D_{50} – median particle diameter; C_u – coefficient of uniformity; C_c – coefficient of curvature).

	G_s [-]	e_{max} [-]	e_{min} [-]	D_{50} [mm]	C_u [-]	C_c [-]
B1	2.65	0.82	0.44	0.317	2.346	0.912
B2	2.65	0.83	0.46	0.244	2.161	0.845

site. Since the interpretation of HPT-MPT tests relies on the assumption of water-saturated soil, it was not attempted to infer k_h values for the unsaturated soil above the water table.

Soil samples were also extracted from the aforementioned boreholes for further characterisation of the soil at the Maasvlakte II site. Visual observation, borehole analysis, and particle size distribution (PSD) tests (see Fig. 8) confirmed the presence of two different sand types, respectively in the upper and lower 5 m of the deposit. Overall, sieving and micrometric analyses revealed that sand, slightly silty and slightly gravelly, with very spherical and moderately round particles, was present down to 10 m below the ground surface. Two distinct batches of soil were created by mixing borehole material associated with either sand type: soil from the upper layer (0–5 m b.g.l.) was used for Batch 1 (B1), while Batch 2 (B2) was made of soil from the lower layer (5–10 m b.g.l.). As reported in Table 2, rather similar index properties were found for B1 and B2 sand samples.

4. Installation tests and pile-soil monitoring

4.1. Field testing programme

As mentioned in the previous section, nine piles in total were used for field testing purposes, namely four MTPs, four ATPs, and one RP, with geometrical specifications reported in Table 3. The distinction between MTPs and ATPs relates to their different roles in the GDP experimental campaign. The ATPs were exploited for preliminary testing of the GDP shaker, so that relevant driving settings could be first adjusted during the installation of non-instrumented test piles. After the installation of the ATPs, it was decided to target for the MTPs axial and torsional vibration frequencies approximately equal to 16.5 Hz and 63 Hz, respectively. The latter pair of values were chosen to exploit as much as possible the vibratory capacity of the GDP shaker, though

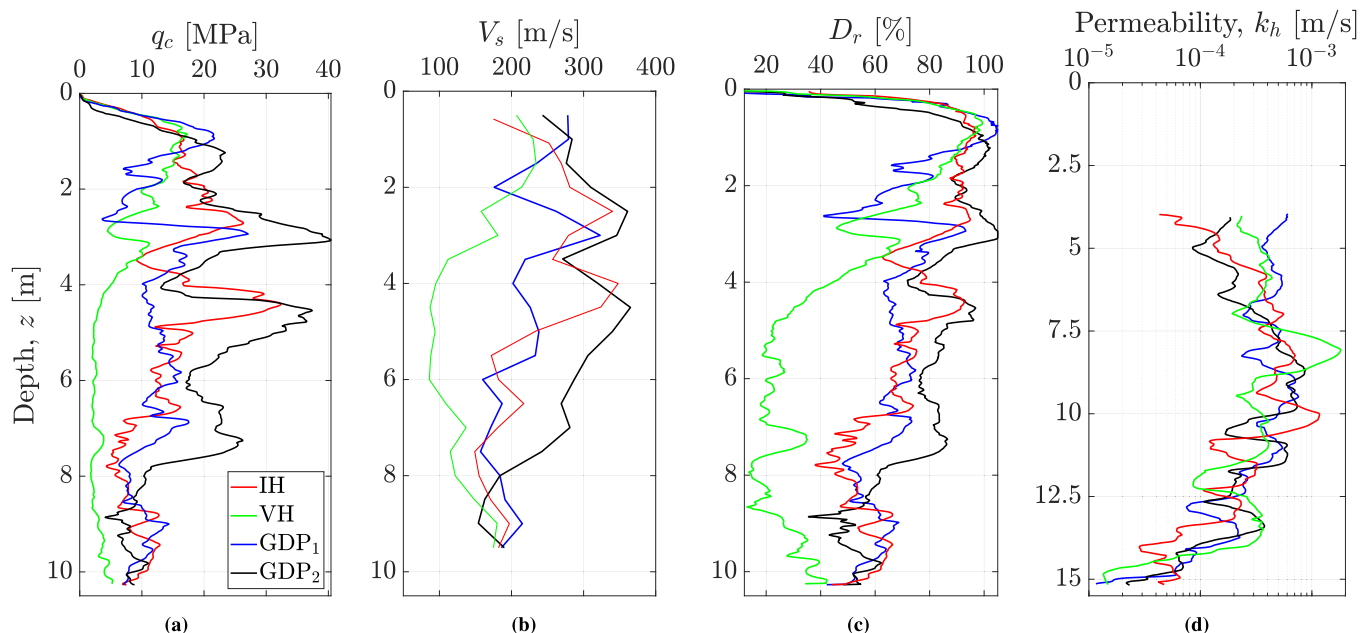


Fig. 7. Profiles of (a) cone resistance (q_c), (b) shear wave velocity (V_s), (c) relative density (D_r), and (d) horizontal hydraulic conductivity (k_h , 80 cm moving average plot) obtained at the MTP locations from in-situ SCPTu and HPT-MPT tests.

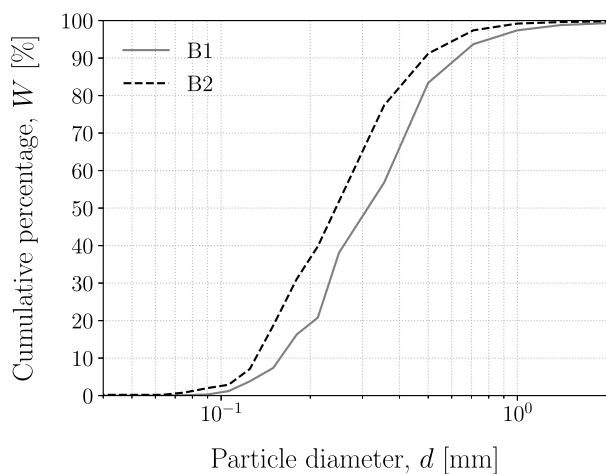


Fig. 8. Particle size distribution (PSD) curves for two representative soil samples from batches B1 and B2.

Table 3
Geometrical characteristics of the piles indicated in Fig. 5.

		Test piles	Reaction pile
Length	L	10 m	10 m
Embedded length	L_e	8 m	8 m
Outer diameter	D	0.762 m	1.6 m
Aspect ratio	L/D	13.12	6.25
Wall thickness	h	0.0159 m	0.02 m

without compromising the testing agenda or operational safety. An axial frequency around 24.8 Hz was adopted for the installation of the VH pile. The ATPs also served post-installation tests, in that they enabled the calibration of specific settings for the subsequent lateral loading tests (Kementzetzidis et al., 2023). Since the main goal of the GDP campaign was to monitor and analyse the performance of the MTPs, they were fully instrumented prior to all tests. This paper presents experimental data that were exclusively recorded on/around the MTPs (mostly for the GDP piles).

Extensive instrumentation of all MTPs and the soil in their surrounding was set in place to monitor the complex soil–pile response during pile driving — see Fig. 5. As previously mentioned, the final pile locations were selected based on the results of the PSI and DSI, with mutual distances limited by the length of the lateral loading frame that was employed afterwards (Kementzetzidis et al., 2023). The circular arrangement shown in Fig. 5 allowed to minimise the interference between consecutive pile driving tests. In chronological order, the MTPs were installed as follows: (i) GDP₂ (30/10/2019), (ii) GDP₁ (30/10/2019), (iii) VH (31/10/2019) and (iv) IH (4/11/2019). The installation sequence may generally be relevant to assessing the interference of consecutive pile installations over a limited soil surface. However, since all pile-to-pile distances were larger than 10D at the GDP test site, it is argued that such interference must have been negligible in all instances (Mabsout et al., 1995; Masoumi et al., 2009).

The same installation protocol was followed for all piles, regardless of the specific driving method. In particular, such a protocol included the following three phases (Fig. 9): (i) in the first phase, the top flange of the pile was connected to the shaker (for VH and GDP piles), then the pile was upended by a crane and positioned vertically at the corresponding installation location. The pile was stabilised by means of lateral restraints, and driven for 0.5 m into the soil. At that point the installation was paused to check that all sensors were functioning properly; (ii) in the second phase, each pile, still laterally restrained, was driven further down to 3 m of total penetration; (iii) in the third phase, lateral restraints were removed and each pile was driven up to the target penetration depth of 8 m. In the remainder of this work only data measured during the third phase of the installation protocol are presented. Such data are believed to be most meaningful in that they relate to pile penetration in water-saturated soil. It is worth noting that both axial and torsional vibration frequencies – and therefore the corresponding load amplitudes (cf. to Eqs. (1)–(2)) – were kept constant during the installation tests.

4.2. Pile instrumentation

During the installation of the MTPs, a number of measurements were performed simultaneously, both on the piles and in the surrounding soil, in order to monitor the dynamic behaviour of the complete



Fig. 9. (a) First, (b) second and (c) third installation phases of an ATP.

pile-soil system. As the GDP method comprises a combination of axial and torsional vibrations, non-zero components of motion in all directions were anticipated. Accordingly, the following sensing instrumentation was deployed:

- two tri-axial micro-electro-mechanical systems (MEMS) accelerometers to record the dynamic motion of the pile during installation. The MEMS accelerometers were positioned 1.56 m below the pile head at diametrically opposite locations (see Fig. 10 and their technical specifications in Table 4);
- fiber Bragg grating (FBG) sensors (12 per side) to monitor pile strains along the length (see specifications in Table 5). The same technology has been recently adopted for pile monitoring during impact driving tests (Buckley et al., 2020). Two types of FBG configurations were adopted, namely in-line FBGs and FBG rosettes (see Fig. 10). In-line FBGs were installed at multiple cross sections along the length, two per cross section at diametrically opposite locations. FBG rosettes were placed at three selected locations along the length, two per cross-section and diametrically opposite, in order to monitor strains along the longitudinal and two inclined directions, at angles of 60° and 120° with respect to the horizontal plane;
- two FBG temperature sensors to measure temperature variations on the pile surface during pile penetration. The main purpose of such measurements was to obtain quantitative factors for temperature compensation of FBG measurements. The temperature sensors were positioned next to the location of the last FBG sensor (approximately 35 cm above the pile tip);
- one potentiometer (draw-wire type) to record the penetration of each pile into the soil by measuring its axial displacement. The measurement range of the potentiometer was ± 10 m and its accuracy equal to 0.1 mm.

All the pile sensors operated at a sampling frequency equal to 1 kHz. Additional details about sensor specifications are provided in Tables 4 and 5. Due to space limitations, only pile measurements obtained from the potentiometer and the MEMS accelerometers are discussed herein.

4.3. Ground monitoring

The response of the soil surrounding the MTPs was monitored during pile driving tests by means of the following ground monitoring instrumentation:

Table 4

Technical specifications of tri-axial MEMS accelerometers.

Type of sensor	MEMS ADXL337
Number of sensors per pile	2 (1 per side)
Measurement range	± 200 g
Bandwidth (x, y axes)	0.5 Hz–1300 Hz
Bandwidth (z axis)	0.5 Hz–1000 Hz
Sensitivity (x axis)	5.8 mV/g
Sensitivity (y axis)	6.5 mV/g
Sensitivity (z axis)	7.2 mV/g

Table 5

Technical specifications of in-line FBG strain sensors.

Type of FBG strain sensor	Sylex FFA-01
Number of sensors per pile	24 (12 per side)
Measurement range	± 3000 $\mu\text{m/m}$
FBG wavelength range	1510 nm–1590 nm
Fiber coating	Polyimide

- Eight VWPC2100 *RST Instruments* sensors containing both soil pressure cells (SPCs) and pore water pressure transducers (PPTs) were deployed to simultaneously record the evolution in time of the total radial stress (σ_r) and the pore pressure (p_w), with accuracy and resolution of 5.0 kPa and 0.25 kPa, respectively. For each MTP and prior to pile driving, the sensors were installed at two different depths (6 m and 8 m below the ground surface, see Fig. 5);
- shape-acceleration arrays (SAAVs) located at the front side of each pile (with respect to the lateral loading direction, Fig. 5) to record lateral soil displacements during installation. The SAAV sensors comprised a cable-shaped series of half-meter rigid segments from 0.5 m to 8.5 m, which would detect lateral soil displacement through the tilt of the individual segments.

After installing the above soil sensors in boreholes dug during the DSI, all SPCs, PPTs, and SAAVs were set to sample data at 1 kHz for all pile installation tests.

Finally, cross-hole sonic logging (CSL) tests were performed before and after pile driving tests, in order to evaluate possible installation effects in the soil by means of P-wave measurements. For these tests, two 10-meter long PVC access tubes were installed at a distance of

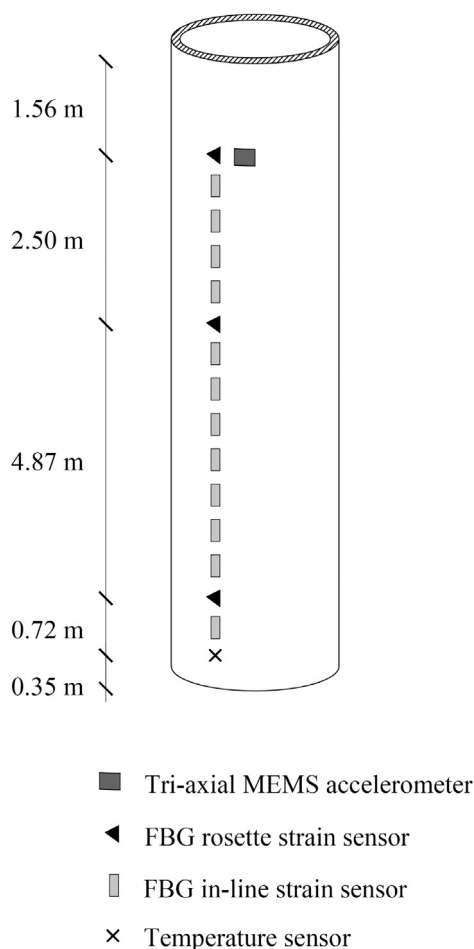


Fig. 10. Pile instrumentation.

0.5 m and 1.5 m from the pile wall (Fig. 5), while two ultrasonic transmitter/receiver probes were lowered to the bottom of the tubes. The transmitted P-waves (50 kHz nominal frequency) were recorded by the receiver probe at a sample rate of 0.5 MHz. To assess repeatability, CSL tests were performed twice for each pile before and after installation.

5. Field observations during GDP installation

This section presents relevant field observations associated with the dynamic response of the MTPs and the surrounding soil during the installation tests — namely, during the third phase of the installation protocol described above. The following analysis of field data is a preliminary effort to demonstrate the potential of the new GDP method, particularly in comparison to standard axial vibratory driving (VH). Due to site inhomogeneity and the inherent differences between the considered driving methods (IH, VH, GDP), further interpretation of the whole dataset may only be achieved through future numerical modelling work.

5.1. Pile penetration rates

Fig. 11 displays the penetration time series for the VH and the two GDP piles. The solid lines correspond to the displacement of GDP₁ and VH as measured by the potentiometer (P), while the respective measurement for GDP₂ is not available due to sensor failure during driving. The markers in the same figure represent the “slow” measurements of the driving logging (DL) system, which includes displacement values recorded every 25 cm of pile penetration. Average penetration rates

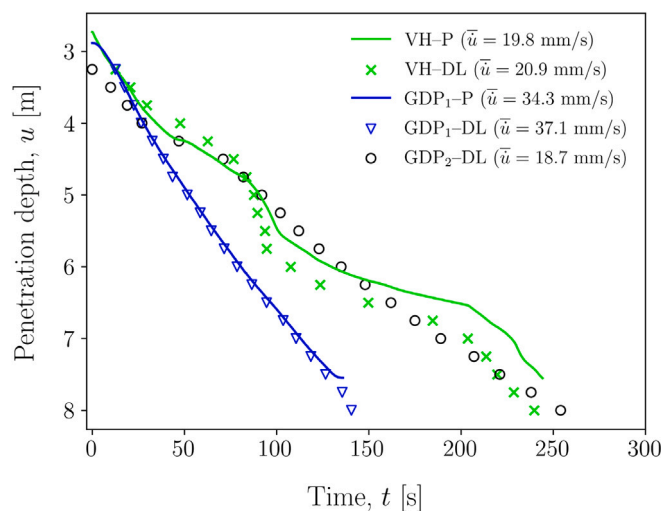


Fig. 11. Pile penetration curves (u) for VH, GDP₁ and GDP₂, with average penetration rates (\bar{u}) obtained from potentiometer (P) and driving log (DL) data.

equal to 20.9 mm/s, 37.1 mm/s and 18.7 mm/s were determined for VH, GDP₁, and GDP₂, respectively, based on the driving logging system; the more reliable data returned by the potentiometer transducer for VH and GDP₁ indicate average penetration rates of 19.8 mm/s and 34.3 mm/s, respectively. The good agreement between the data from the potentiometer and the driving log led to consider the latter reliable also for GDP₂'s installation.

As can be observed in Fig. 11, GDP₁ had a shorter installation time compared to VH and GDP₂ (and therefore a larger penetration rate). Since the two GDP piles were driven with identical installation settings, GDP₁'s higher installation rate was presumably due to the lower cone resistance (q_c) and relative density (D_r) at the corresponding soil location — see Fig. 7. Although VH was installed in weaker soil, GDP₁ penetrated at an almost double average rate. Further, while GDP₂ was driven into the strongest soil (among the four MTP locations), its average penetration rate was found to be very similar to VH's (Fig. 11). These facts seem to support that combining axial and torsional vibrations was indeed beneficial from a pile driving perspective.

It was also possible to obtain more detailed information about the penetration rates by numerically differentiating the pile penetration time series — which could be done using the potentiometer data, therefore only for VH and GDP₁. The differentiated time series are given in Figs. 12(a)–12(b) alongside their low-pass filtered counterparts (a moving average filter with a cut-off frequency of 2 Hz). Fig. 12(b) indicates that GDP₁'s penetration rate was on average fairly constant during installation. In contrast, VH penetrated at a more variable rate, with some abrupt changes during the penetration process — see, e.g., the spike around 100 s. Considering the penetration depth reached by VH's tip after such time (between 4 and 5 m), it is likely that the transition from unsaturated to saturated soil had a temporary influence on the penetration rate. It is again apparent that GDP₁'s driving outperformed VH's, especially considering that the latter was installed in weaker soil (Fig. 7). Overall, the penetration rates observed at the GDP site resemble quite closely the (high) values reported by Whenham (2011) during the axial vibro-driving of similarly sized open-ended pipe piles. Importantly, no refusal was experienced during GDP driving, as is testified by the rather steady penetration rates in Fig. 11.

5.2. Power and energy consumption

In addition to pile penetration measurements, the power consumption of the GDP shaker and the axial vibro-hammer was also monitored

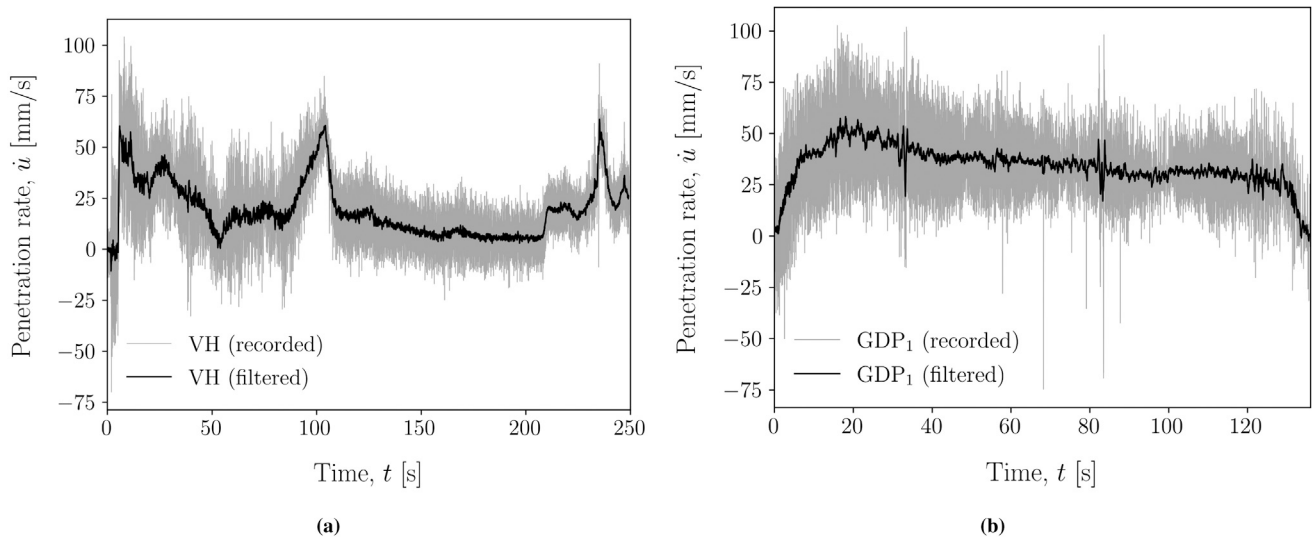


Fig. 12. Time evolution of the pile penetration rate (\dot{u}) obtained for (a) VH and (b) GDP₁ from potentiometer (P) data.

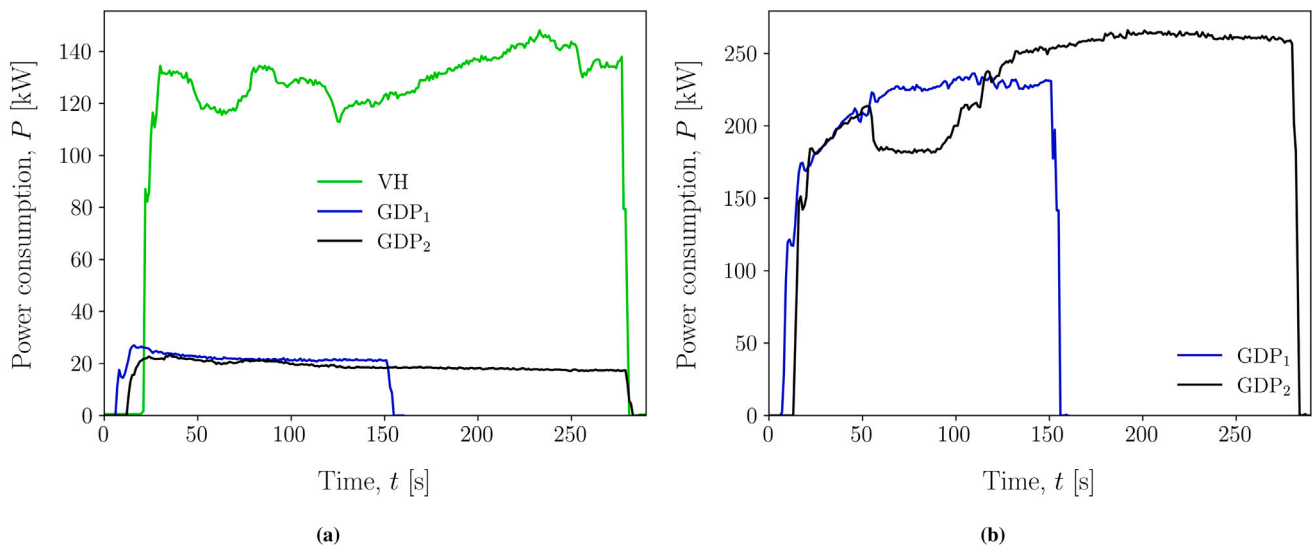


Fig. 13. HPU power consumption (P) associated with (a) axial and (b) torsional loads applied to VH, GDP₁, and GDP₂.

to assess the efficiency of the different methods. In agreement with the GDP shaker specifications in Table 1, two independent exciter blocks were used for the axial and the torsional excitation. In Fig. 13(a), the HPU power consumption is plotted against time for the axial excitation provided by the GDP shaker and the axial vibro-hammer; the torsional HPU power consumption is shown in Fig. 13(b), exclusively for the two GDP piles.

It is readily apparent that the power consumed to impose torsional vibrations is substantially larger than its axial counterpart for both GDP₁ and GDP₂. Generally, the HPU power consumed for axial loading of both GDP piles was found to be almost identical, and significantly lower than the power consumed to axially vibrate the VH pile (Fig. 13(a)). In contrast, the power associated with the torsional loading of the GDP piles is larger than that consumed for the VH pile, as one would expect in light of the higher frequency of torsion. Overall, the power consumed by the GDP shaker lies inside the power capacity of the VH device, as was indeed a target of the first GDP shaker design to enable fair comparisons.

It is also worth noting that GDP₂ consumed through torsion more power than GDP₁, as a likely outcome of the denser soil profile at the GDP₂ location — this is also confirmed by the longer installation time

(Fig. 13(b)). Further, a drop in torsional power consumption is visible for GDP₂ between 50 s to 100 s: since power was delivered to maintain a given vibration frequency (which was constant during driving), a local reduction in soil resistance may have caused a temporary power drop of the kind shown in Fig. 13(b). As time elapsed, the power consumed to axially vibrate both GDP piles slightly decreased with the penetration depth, while the torsional power tended to increase in time for both piles. Overall, these trends indicate that the soil resistance to pile driving was mainly overcome through the torsional mechanism. This observation strongly supports the conceptual foundation of GDP driving, i.e., the beneficial effect of torsional vibrations in overcoming the frictional soil resistance along the pile shaft.

As a final comparison between VH and GDP driving performances, the total energy consumption (both axial and torsional for GDP) is plotted against the installation time in Fig. 14. The efficiency of the GDP method is clearly supported by the fact that GDP₁ consumed approximately the same total energy as VH (only 2.8% larger), even though GDP₁ was driven in substantially stronger soil. On the other hand, GDP₂ required approximately twice as much energy as needed for GDP₁, which was mostly due to the stronger soil encountered at that location (Fig. 7). A detailed discussion of energy efficiency matters and

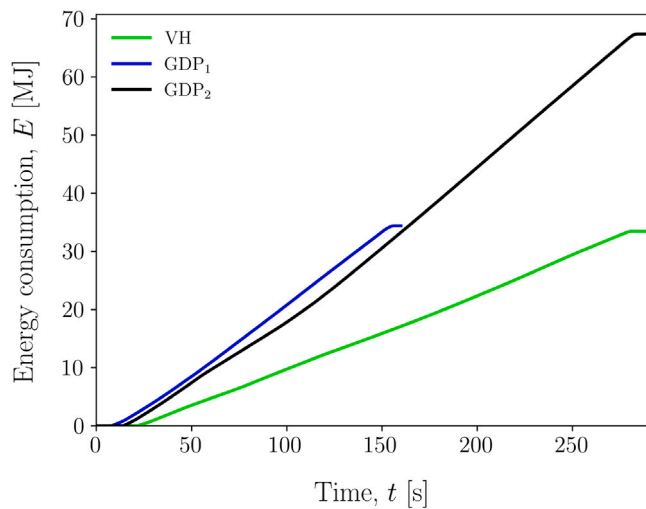


Fig. 14. Time evolution of the total energy consumption (E) during the installation of VH, GDP₁, and GDP₂ (both axial and torsional components included for GDP-driven piles).

Table 6

Comparison of geotechnical properties and driving performance for VH, GDP₁, and GDP₂.

	VH	GDP ₁	GDP ₂
Average cone resistance, \bar{q}_c	5.75 MPa	11.9 MPa	18.6 MPa
Total energy consumption, E	33.44 MJ	34.39 MJ	67.38 MJ
Average penetration rate, \bar{u}	19.8 mm/s	34.3 mm/s	18.7 mm/s

their quantification both for VH and GDP piles is provided by Gómez et al. (2022). For clarity, the values of average cone resistance along the soil profile, total energy consumption, and the average penetration rate are summarised in Table 6 for VH, GDP₁, and GDP₂.

5.3. Pile response during driving

To portray relevant features of the dynamic pile response during GDP driving, acceleration spectra have been obtained from the output of the two MEMS accelerometers. In particular, the amplitudes of the acceleration spectra are shown in Fig. 15 both for GDP₁ and GDP₂, and each spatial direction, i.e., $|a_z|$ (axial), $|a_r|$ (radial), and $|a_\theta|$ (circumferential). The driving frequency of the GDP shaker in the axial direction was measured at 16.3 Hz and 16.5 Hz for piles GDP₁ and GDP₂, respectively. These frequencies correspond to well-visible peaks in Figs. 15(a)–15(b) (grey dashed lines). Next to these primary amplitude peaks, which are directly related to the main driving frequencies, the pile response is amplified at multiple other harmonics. The reason for this observation is twofold. First, the shaker itself excites the system at multiple super-harmonics (of the main driving frequency) due to minor imperfections in the rotation of the eccentric masses. This statement applies to both vibration modes excited in the pile, i.e., axial and torsional. Secondly, the dynamic response of the system is inherently non-linear even at low vibration amplitudes, and this fact may cause further amplification of the mentioned super-harmonics (Rega et al., 1991). The extent to which each of these two mechanisms contributes to the energy content in the super-harmonics has not been quantified — however, the first mechanism is believed to be dominant. It is also interesting to note that frequencies (including super-harmonics) associated with the torsional vibration are clearly visible in the other acceleration spectra. By comparing the spectra in Fig. 15 for the two GDP piles, it can be stated that the acceleration response is almost identical regardless of moderately different soil conditions, which indicates strong dependence on the GDP excitation.

The amplitudes of the circumferential acceleration spectra ($|a_\theta|$) show for both GDP piles a distinct peak at the main torsional driving frequency, i.e., at 62.6 Hz and 63 Hz for piles GDP₁ and GDP₂, respectively. Once again, the frequencies of 125 Hz and 188 Hz (approximately), corresponding to the first and second super-harmonics, are associated with prominent spectral amplitudes.

The acceleration spectra in Fig. 15 provide a detailed picture of the frequency content during the time interval taken into account. Such an interval was chosen to be a 10 s time window approximately in the middle of the third driving phase. Such a choice was motivated by the abrupt variation in frequency content at the beginning and the end of the driving process, due to the (de)activation of the GDP shaker. It is however worth recalling that the acceleration signals recorded during pile penetration may not be *a priori* regarded as stationary. In Figs. 16–17 the discrete short-time Fourier transforms (STFTs) of the sensor-averaged pile accelerations are shown in spectrogram form (Brandt, 2011) for the axial and circumferential components of motion, which are the most relevant to the GDP vibratory excitation. In the resulting time–frequency analysis, a trade-off between resolution in time and frequency had to be found, as a consequence of the Gabor limit (Gabor, 1946).

Fig. 16 confirms that the frequency content was relatively constant during the main part of the installation (phase three), as was to be expected based on the installation settings (constant frequency) and the steady pile penetration trends observed in Fig. 11. The existence of the previously identified super-harmonics is confirmed throughout the whole installation process. For GDP₁, Fig. 16(a) shows that the super-harmonics associated with the axial driving frequency slightly decreased in amplitude towards the end of driving — conversely, this observation does not apply to the main driving frequency above 16 Hz and its first super-harmonic at 33 Hz, which seem to have maintained a fairly constant amplitude. The amplitude of the frequency component close to the torsional excitation frequency decreased significantly towards the end of driving.

The results of the time–frequency analysis performed for the circumferential acceleration signals are reported in Fig. 17. In this case the main driving frequency is clearly apparent, and its energy level is considerably larger than that associated with the super-harmonics. This is in full agreement with what has been observed about Fig. 15. The amplification of the second torsional super-harmonic towards the end of GDP₂'s installation is further supported by Fig. 17(b). Similarly to the case of the axial acceleration (Fig. 16), the spectrogram of the circumferential acceleration (Fig. 17) corroborates that the torsional driving frequency (and the associated amplitude) remained nearly constant during GDP installation, as per the intended installation settings.

5.4. Ground monitoring data

Further insight into the mechanics of GDP can be obtained by inspecting ground monitoring data. In Fig. 18, pore water pressure variations Δp_w (with respect to local, pre-installation values) are plotted against time for both GDP piles and at two different depths (6 m and 8 m below the ground surface). The vertical lines in all subplots of Fig. 18 indicate the times when the pile reaches a penetration depth of 6 m (location of the first PPT) and 8 m (location of the second PPT and target penetration depth). A common feature of all Δp_w trends in Fig. 18 is the gradual increase in pore water pressure during driving, which is consistent with previous observations regarding vibratory driving in saturated granular soils (Holeyman, 2002). Subsequently, excess pore pressures attenuate as pile driving reaches its conclusion: pore pressure dissipation takes only a few minutes in a soil as permeable as that at the Maasvlakte site. The outlook of Fig. 18(a) (for GDP₁) and Fig. 18(b) (for GDP₂) reveals maximum pore pressure variations in the order of 10 kPa for both piles and reference depths, although larger Δp_w emerge for the pile installed in denser soil (GDP₂). A sudden increase in pore water pressure is visible at 60 s (approximately 4 m penetration), followed

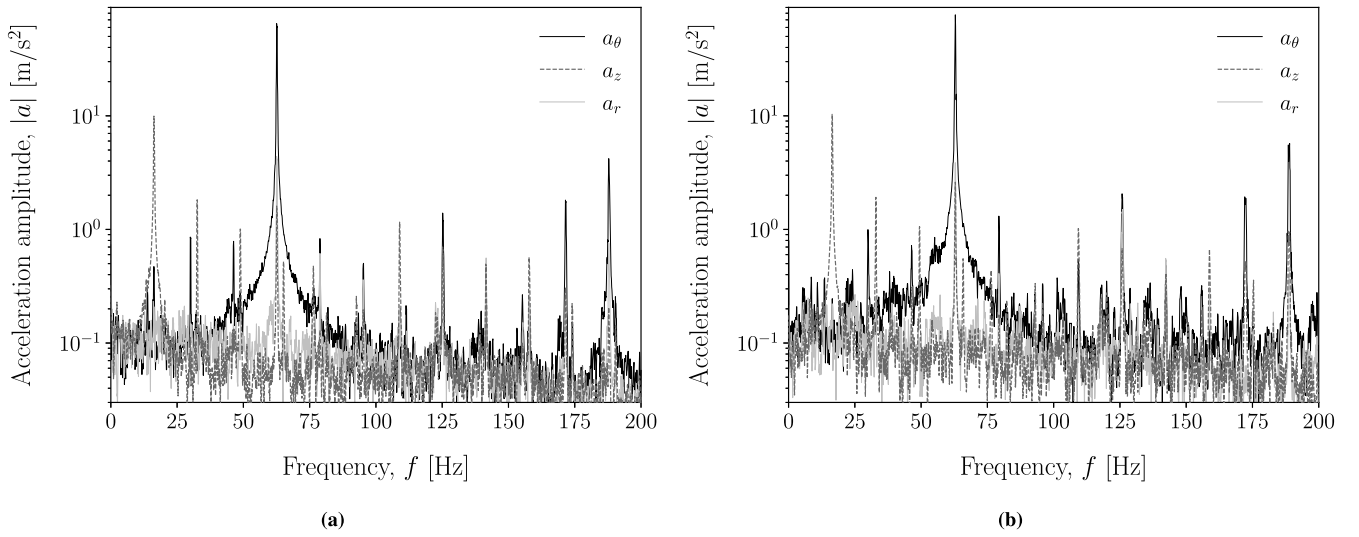


Fig. 15. Amplitude of acceleration spectra in all directions for piles (a) GDP₁ and (b) GDP₂.

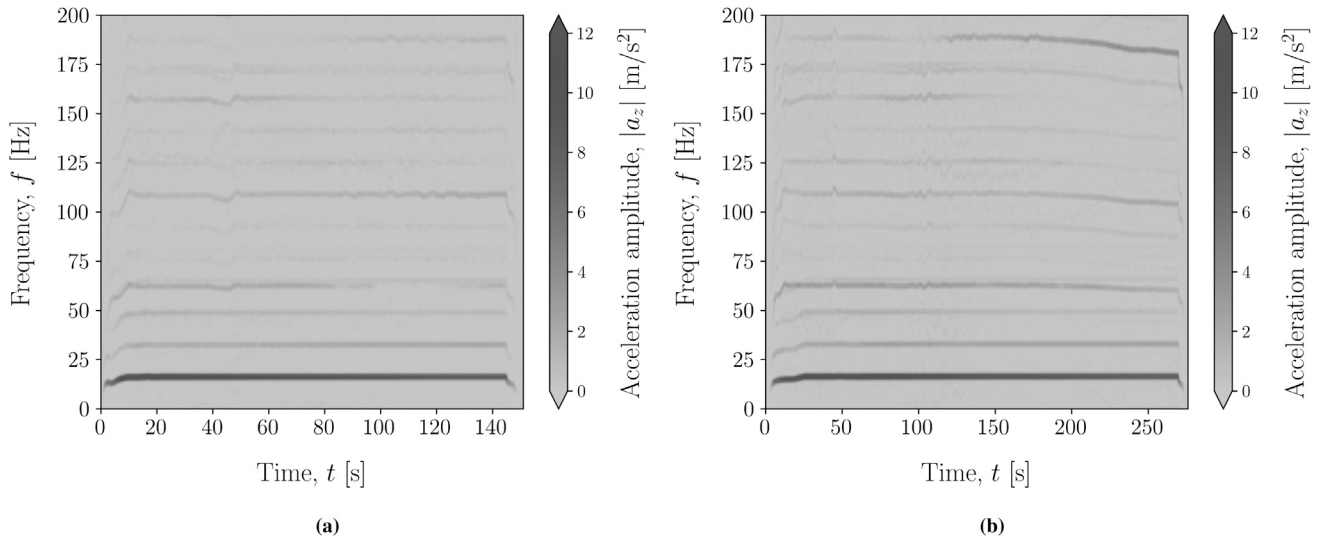


Fig. 16. Amplitude of the STFT in axial direction $|a_z|$ for (a) GDP₁ and (b) GDP₂.

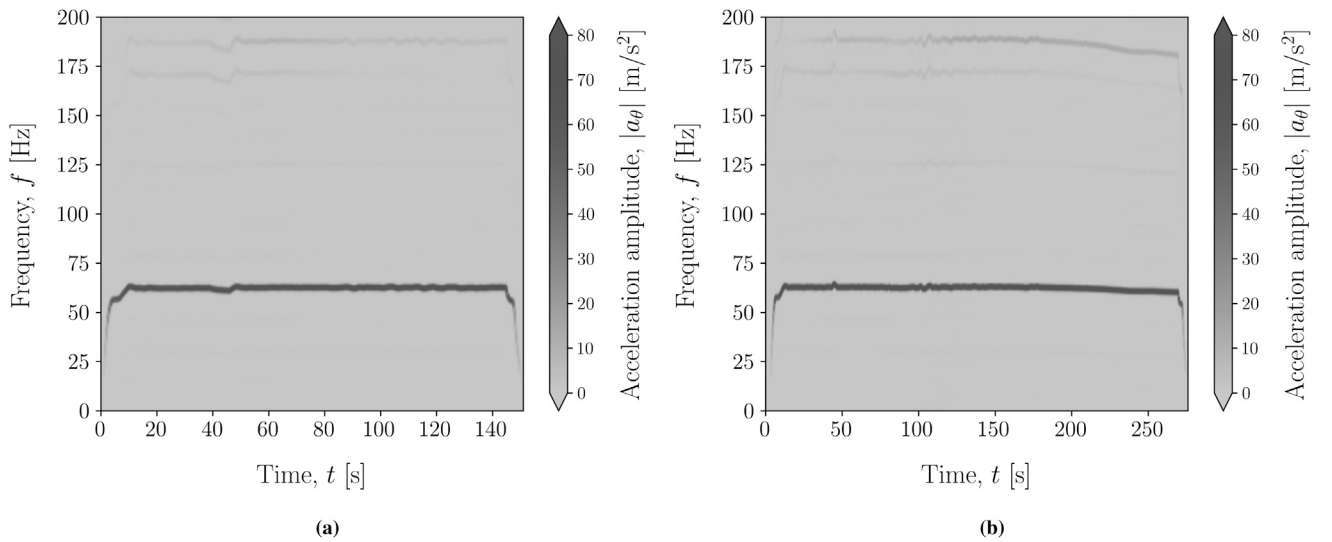


Fig. 17. Amplitude of the STFT in circumferential direction $|a_\theta|$ for (a) GDP₁ and (b) GDP₂.

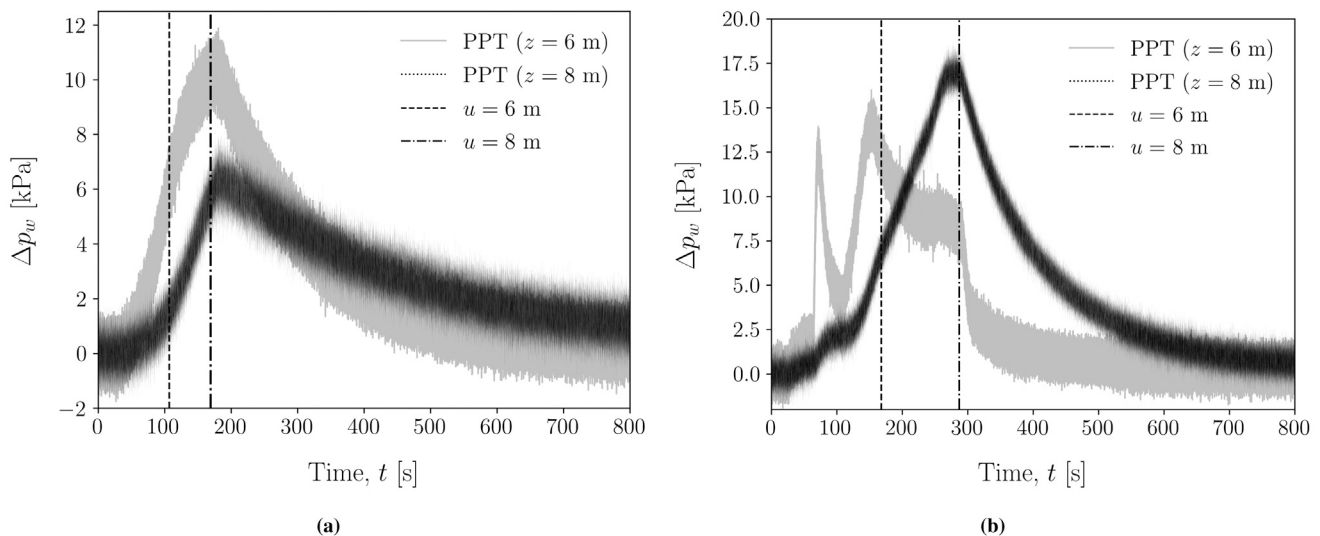


Fig. 18. Pore water pressure variations (Δp_w) recorded during the installation of (a) GDP₁ and (b) GDP₂ at depths, z , equal to 6 m and 8 m below the ground surface. The vertical dashed lines indicate the times when the pile tip penetration (u) equals the depths of the two PPT sensors.

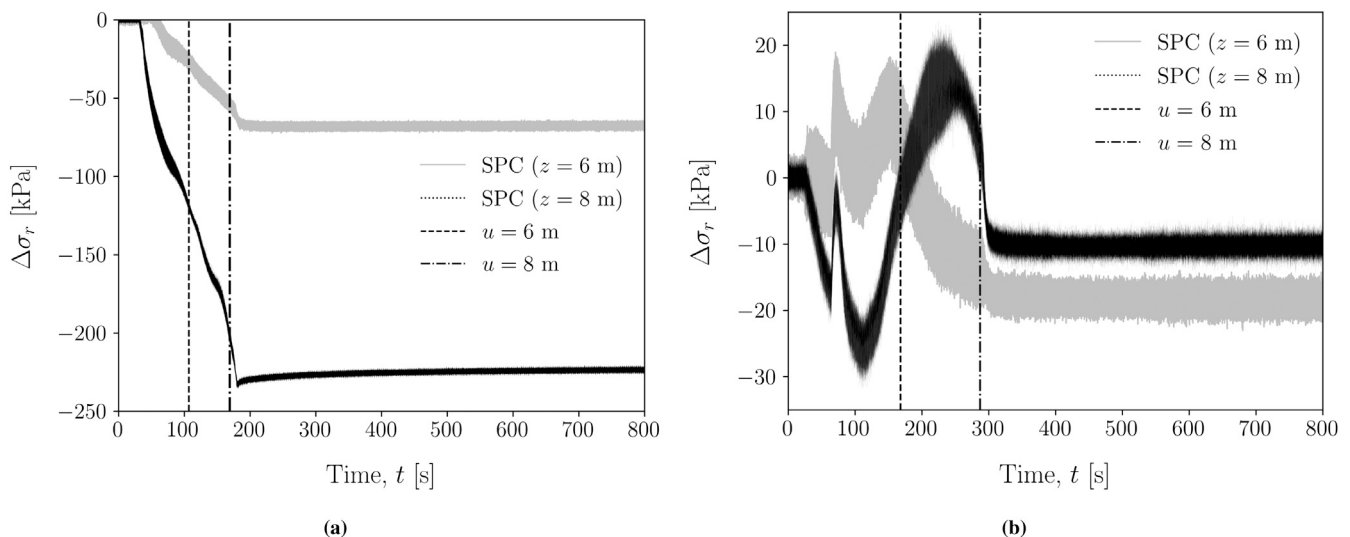


Fig. 19. Total radial soil stress variations ($\Delta \sigma_r$) recorded during the installation of (a) GDP₁ and (b) GDP₂ at depths, z , equal to 6 m and 8 m below the ground surface. The vertical dashed lines indicate the times when the pile tip penetration (u) equals the depths of the two SPC sensors.

by a temporary drop in excess pore pressure at $z = 6$ m in Fig. 18(b). The former increase may be attributed to a local inhomogeneity in the GDP₂ soil profile between 3 m and 5 m – cf. to the q_c profile in Fig. 7(a) – while the ensuing drop seems to be closely related to the decrease in torsional power consumption (and therefore in mobilisation of soil resistance) that has been previously observed for GDP₂ in Fig. 13. Fig. 18(b) does not show a similar behaviour at $z = 8$ m, which may be due to the larger distance of the PPT from the pile tip during the relevant time interval.

At the same depths where pore water pressures were measured, variations in total horizontal/radial soil stresses ($\Delta \sigma_r$) were also monitored – see Fig. 19. The soil pressure measurements for GDP₂ in Fig. 19(b) show different trends at the two reference depths. Nonetheless, $\Delta \sigma_r$ evolves to reach soil pressures lower than the estimated pre-installation values both at 6 m and 8 m below the ground surface – more prominently at the shallower location ($z = 6$ m). The overall reduction in radial (total) confinement is likely associated with vibration-induced sand densification. Such a densification is indeed expected to be more significant at shallower soil locations, i.e., where the soil experiences a larger number of dynamic loading cycles.

As for $\Delta \sigma_r$ measurements around GDP₁, it should be noted that a significantly larger reduction was measured for no obvious reason – see Fig. 19(a). Although decreasing $\Delta \sigma_r$ is consistently found in both GDP piles, full reliability of soil pressure data around GDP₁ may not be taken granted. In principle, the stiffness of the SPCs should be similar to the soil stiffness to avoid arching effects and properly capture soil stress conditions. A number of factors, such as local soil inhomogeneity and/or sensor installation in a soil of quite different stiffness, might have produced inaccuracies in the measured data.

It was also decided not to report herein SAAV measurements of soil displacement, since the sensors recorded displacement values that were lower than the sensor accuracy.

5.5. Impact of GDP driving on soil stiffness

During the PSI and the DSI, well-established in-situ procedures such as CPTu, SCPtu, and HPT-MPT were performed. However, it was the first time – to the authors' knowledge – that CSL tests were planned for geotechnical investigation purposes (CSL tests are most usually performed to detect mechanical anomalies in drilled shafts and diaphragm

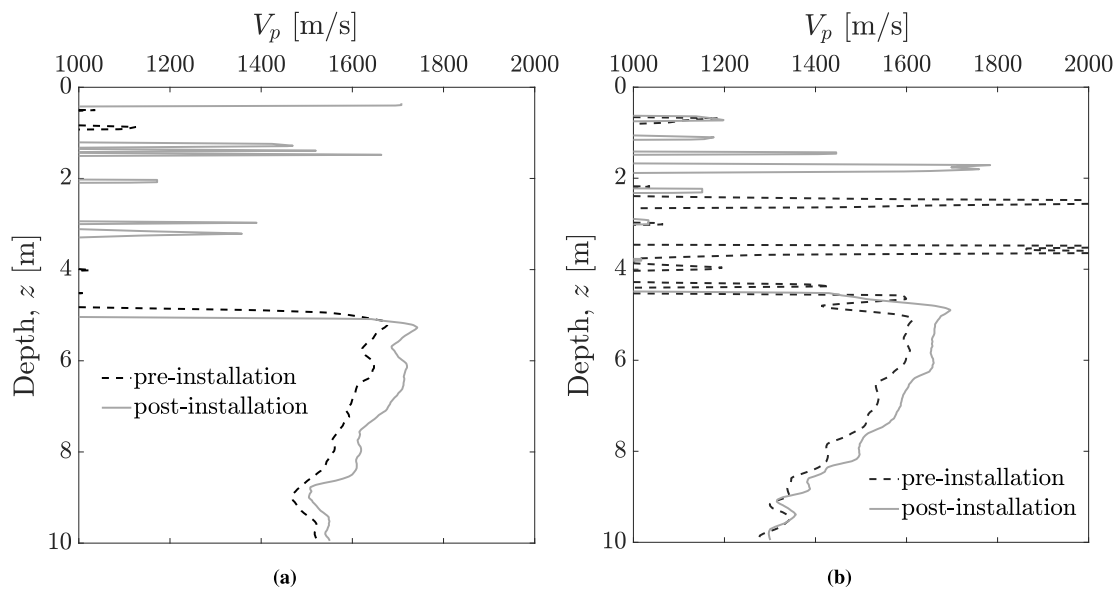


Fig. 20. CSL test results: V_p profiles obtained before (solid lines) and after (dashed lines) pile installation in the vicinity of (a) GDP₁ and (b) GDP₂.

walls Spruit et al., 2014). Specifically, CSL tests were performed before and after pile installation to evaluate the impact of GDP driving on the stiffness of the surrounding soil. Since compression wave velocity V_p is related to the stiffness of the medium, variations in wave velocity can be used for general quantification of installation effects. Depth-profiles of average compression wave velocity (tests were performed twice) before and after pile installation are reported in Fig. 20. The V_p profiles in the upper soil layers exhibit significant scatter, and are generally unreliable as a consequence of unsaturated soil conditions. Conversely, deeper V_p measurements appear to be reliable and in agreement with expectations. In particular, appreciable V_p enhancement can be observed in the lower water-saturated soil, which indicates an overall stiffening of the soil around the pile. This finding is consistent with the $\Delta\sigma_r$ trends shown in Fig. 19, and reinforces the belief that GDP driving can induce soil densification/stiffening with no apparent evidence of soil degradation.

6. Concluding remarks

Recent research related to the GDP project ('Gentle Driving of Piles') has been presented in this paper, which is a companion to the study by Kementzetzidis et al. (2023). GDP is a TU Delft-led joint industry project on the development of a new vibratory driving technology for monopiles. Its stepping stone is the idea that both efficient installation and low noise emission can be achieved by applying to the pile a combination of low-frequency/axial and high-frequency/torsional vibrations. To achieve a first demonstration of the GDP concept, medium-scale field tests were performed at the sandy Maasvlakte II site in Rotterdam. Such tests included installation experiments with different driving methods (impact hammering, axial vibro-driving, and GDP), followed by cyclic/dynamic loading of the same piles.

The main experimental evidence presented in this paper may be summarised as follows:

- two test piles have been smoothly installed at the reference site via GDP driving, with fairly constant/high penetration rates and no instances of pile refusal;
- the comparison between GDP and axial vibro-installation has highlighted the remarkable potential of the GDP method. Compared to standard axial vibro-driving, the GDP method enabled faster installation in stiffer soil with comparable total energy consumption (cf. GDP₁'s installation data to VH's);

- the values of HPU power consumed to impose axial and torsional vibrations have proven consistent with typical magnitude levels for vibro-piling. Particularly, the evolution in time of such power values has suggested that the torsional mechanism contributed the most to pile penetration;
- the frequency and time-frequency analyses of pile acceleration signals have indicated that frequencies mainly associated with the vibrations of the GDP shaker were excited during driving, which has turned out to be a nearly stationary process under the reference site conditions;
- the hydro-mechanical response of the soil during driving has been found to be in line with expectations for vibratory driving processes. Pore pressures in the order of a few kPa built up and rapidly dissipated in the permeable soil at hand. A gradual relaxation in the total radial soil stress has been observed as a likely outcome of vibration-induced soil densification;
- the results of in-situ CSL tests have shown an increase in soil's P-wave velocity after pile installation, which may be associated with an overall increase in soil stiffness due to the mentioned densification.

The field campaign has preliminarily demonstrated the potential of the GDP method as an efficient and 'silent' pile installation technology. The results presented in this paper, along with those regarding the post-installation performance of the test piles (see the companion paper), encourage further development of the proposed piling approach. More quantitative analysis of all installation test results will be presented in the future after detailed numerical modelling work.

CRediT authorship contribution statement

Athanasios Tsetas: Conceptualization, Methodology, Software, Formal analysis, Investigation, Data curation, Writing – original draft. **Apostolos Tsouvalas:** Conceptualization, Methodology, Writing – review & editing, Supervision, Project administration, Funding acquisition. **Sergio S. Gómez:** Conceptualization, Methodology, Software, Formal analysis, Investigation, Data curation, Writing – original draft, Project administration. **Federico Pisanò:** Conceptualization, Methodology, Writing – original draft, Supervision, Project administration. **Evangelos Kementzetzidis:** Conceptualization, Methodology, Software, Data curation, Writing – original draft. **Timo Molenkamp:** Software, Investigation, Data curation. **Ahmed**

S.K. Elkadi: Writing – original draft, Project administration. **Andrei V. Metrikine:** Conceptualization, Methodology, Writing – review & editing, Supervision, Project administration, Funding acquisition.

Declaration of competing interest

The authors declare that they have no known competing financial interests or personal relationships that could have appeared to influence the work reported in this paper.

Data availability

Some data may be made available upon reasonable request to the corresponding author, after approval of all GDP project partners.

Acknowledgements

This paper is associated with the GDP project in the framework of the GROW joint research program. Funding from Topsector Energiesubsidie van het Ministerie van Economische Zaken under grant number TEHE117100 and financial/technical support from the following partners is gratefully acknowledged: Royal Boskalis Westminster N.V., CAPE Holland B.V., Deltares, Delft Offshore Turbine B.V., Delft University of Technology, ECN, Eneco Wind B.V., IHC IQIP B.V., RWE Offshore Wind Netherlands B.V., SHL Offshore Contractors B.V., Shell Global Solutions International B.V., Sif Netherlands B.V., TNO, and Van Oord Offshore Wind Projects B.V. The important contribution to the GDP field campaign of, in alphabetical order, Rob Atkinson, Kees van Beek, Maxim L.A. Segeren, Faraz S. Tehrani, Peter de Vries, is also warmly appreciated.

References

- Achmus, M., Schmoor, K.A., Herwig, V., Matlock, B., 2020. Lateral bearing behaviour of vibro-and impact-driven large-diameter piles in dense sand. *Geotechnik* 43 (3), 147–159.
- Anusic, I., Lehane, B., Eiksund, G., Liingaard, M., 2019. Influence of installation method on static lateral response of displacement piles in sand. *Géotech. Lett.* 9 (3), 193–197.
- Barkan, D., 1967. Developments in soil dynamics. In: *Proceedings International Symposium on Wave Propagation and Dynamic Properties of Earth Materials*. University of New Mexico Press, Albuquerque, New Mexico.
- Brandt, A., 2011. *Noise and Vibration Analysis: Signal Analysis and Experimental Procedures*. John Wiley & Sons.
- Buckley, R.M., McAdam, R.A., Byrne, B.W., Doherty, J.P., Jardine, R.J., Kontoe, S., Randolph, M.F., 2020. Optimization of impact pile driving using optical fiber Bragg-Grating measurements. *J. Geotech. Geoenviron. Eng.* 146 (9), 04020082.
- Byrne, B.W., Aghakouchak, A., Buckley, R.M., Burd, H.J., Gengenbach, J., Houlsby, G.T., McAdam, R.A., Martin, C.M., Schranz, F., Sheil, B.B., Suryasentana, S.K., 2020. PICASO: Cyclic lateral loading of offshore wind turbine monopiles. In: Westgate, Z. (Ed.), *Frontiers in Offshore Geotechnics IV: Proceedings of the 4th International Symposium on Frontiers in Offshore Geotechnics*. ISFOG 2021. Houston, TX, USA, CRC Press/Balkema, Leiden, the Netherlands, pp. 1526–1535.
- Byrne, B.W., Burd, H.J., Zdravkovic, L., Abadie, C.N., Houlsby, G.T., Jardine, R.J., Martin, C.M., McAdam, R.A., Pacheco Andrade, M., Pedro, A.M., et al., 2019. PISA design methods for offshore wind turbine monopiles. In: *Offshore Technology Conference*. Offshore Technology Conference.
- De Nicola, A., Randolph, M.F., 1993. Tensile and compressive shaft capacity of piles in sand. *J. Geotech. Eng.* 119 (12), 1952–1973.
- European Commission, 2020. Offshore renewable energy strategy. <https://ec.europa.eu/info/law/better-regulation/have-your-say/initiatives/12517-Offshore-renewable-energy-strategy>. (Accessed 21 September 2020).
- Forsberg, K., 1969. Axisymmetric and beam-type vibrations of thin cylindrical shells. *AIAA J.* 7 (2), 221–227.
- Gabor, D., 1946. Theory of communication. Part I: The analysis of information. *J. Inst. Electr. Eng. III Radio Commun. Eng.* 93 (26), 429–441.
- Georgiadis, M., Saffekou, S., 1990. Piles under axial and torsional loads. *Comput. Geotech.* 9 (4), 291–305.
- Gómez, S.S., Metrikine, A.V., 2021. Shaker for gentle driving of piles. <https://patentscope.wipo.int/search/en/detail.jsf?docId=WO2021040523&tab=PCTBIBLIO>.
- Gómez, S.S., Tsetas, A., Metrikine, A.V., 2022. Energy flux analysis for quantification of vibratory pile driving efficiency. *J. Sound Vib.* 541, 117299.
- Herwig, V., Gattermann, J., 2015. VIBRO-project–Vergleich der lateralen Tragfähigkeit von vibrierten und geschlagenen Stahlpfählen in sandigen Böden. In: *Pfahl-Symposium*, Vol. 19, No. 20.02. p. 2015.
- Holeyman, A.E., 2002. Soil behavior under vibratory driving. In: *Proceedings of the International Conference on Vibratory Pile Driving and Deep Soil Compaction*, Transvib 2002. pp. 3–19.
- IQIP, I., 2020. IHC IQIP takes next step in development blue piling technology. <https://www.ihciqip.com/en/news/ihc-iqip-takes-next-step-in-development-of-blue-piling-technology>. (Accessed 11 January 2021).
- Jamiolkowski, M., Lo Presti, D., Manassero, M., 2003. Evaluation of relative density and shear strength of sands from CPT and DMT. In: *Soil Behavior and Soft Ground Construction*. pp. 201–238.
- Jensen, F.B., Kuperman, W.A., Porter, M.B., Schmidt, H., 2011. *Computational Ocean Acoustics*. Springer Science & Business Media.
- Kallehave, D., Byrne, B.W., LeBlanc Thilsted, C., Mikkelsen, K.K., 2015. Optimization of monopiles for offshore wind turbines. *Phil. Trans. R. Soc. A* 373 (2035), 20140100.
- Kausel, E., 2006. *Fundamental Solutions in Elastodynamics: A Compendium*. Cambridge University Press.
- Kementzetzidis, E., Pisanò, F., Elkadi, A., Tsouvalas, A., Metrikine, A., 2023. Gentle driving of piles (gdp) at a sandy site combining axial and torsional vibrations: part II - cyclic/dynamic lateral loading tests. *Ocean Eng.*
- Koschinski, S., Lüdemann, K., 2013. Development of noise mitigation measures in offshore wind farm construction. pp. 1–102, Commissioned By the Federal Agency for Nature Conservation.
- Mabsout, M.E., Reese, L.C., Tassoulas, J.L., 1995. Study of pile driving by finite-element method. *J. Geotech. Eng.* 121 (7), 535–543.
- Masoumi, H.R., François, S., Degrande, G., 2009. A non-linear coupled finite element-boundary element model for the prediction of vibrations due to vibratory and impact pile driving. *Int. J. Numer. Anal. Methods Geomech.* 33 (2), 245–274.
- Mazza, N., Holeyman, A., 2019. Frequency-penetration response spectrum on vibratory amplitude matching of monopiles. In: *10th International Conference on Stress Wave Theory and Testing Methods for Deep Foundations*. ASTM International, pp. 468–492.
- Meijers, P., Tsouvalas, A., Metrikine, A., 2018. A non-collocated method to quantify plastic deformation caused by impact pile driving. *Int. J. Mech. Sci.* 148, 1–8.
- Metrikine, A., Tsouvalas, A., Segeren, M., Elkadi, A., Tehrani, F., Gómez, S., Atkinson, R., Pisanò, F., Kementzetzidis, E., Tsetas, A., Molenkamp, T., van Beek, K., P., D., 2020. GDP: a new technology for gentle driving of (mono) piles. In: Westgate, Z. (Ed.), *Frontiers in Offshore Geotechnics IV: Proceedings of the 4th International Symposium on Frontiers in Offshore Geotechnics*. ISFOG 2021 Austin, TX, USA, CRC Press/Balkema, Leiden, the Netherlands, pp. 736–745.
- Minister of Economic Affairs and Climate Policy, 2020. Offshore Wind Energy Roadmap 2030. <https://www.government.nl/topics/renewable-energy/documents/parliamentary-documents/2018/03/27/letter-to-parliament-offshore-wind-energy-roadmap-2030>. (Accessed 11 September 2020).
- Mosher, R.L., 1987. Comparison of Axial Capacity of Vibratory-Driven Piles to Impact-Driven Piles. Technical Report, Engineer Research and Development Center (ERDC).
- Mosher, R.L., 1990. Axial capacity of vibratory-driven piles versus impact-driven piles. *Transp. Res. Rec.* (1277).
- OpenStreetMap contributors, 2017. Planet dump retrieved from <https://planet.osm.org>. <https://www.openstreetmap.org>.
- Page, A.M., Klinkvort, R.T., Bayton, S., Zhang, Y., Jostad, H.P., 2020. A procedure for predicting the permanent rotation of monopiles in sand supporting offshore wind turbines. *Mar. Struct.* 75, 102813.
- Page, A.M., Norén-Cosgriff, K., Skau, K.S., Kaynia, A.M., 2019. REDWIN foundation models for integrated dynamic analyses of offshore wind turbines. In: *International Conference on Offshore Mechanics and Arctic Engineering*, Vol. 58899. American Society of Mechanical Engineers, V010T09A073.
- Pisanò, F., Askarnejad, A., Wang, H., Maghsoodi, S., Gavin, K.G., Segeren, M.L.A., Elkadi, A.S.K., de Lange, D., Konstadinou, M., 2022. MIDAS: Monopile improved design through advanced cyclic soil modelling. In: *Proceedings of 20th International Conference on Soil Mechanics and Geotechnical Engineering*. ICSMGE2022. Sydney, Australia.
- Ramírez, L., Fraile, D., Brindley, G., 2021. Offshore wind in Europe: Key trends and statistics 2020. *WindEurope*.
- Rega, G., Benedetti, F., Salvatori, A., 1991. Periodic and chaotic motions of an unsymmetrical oscillator in nonlinear structural dynamics. *Chaos Solitons Fractals* 1 (1), 39–54.
- Robertson, P.K., 1990. Soil classification using the cone penetration test. *Can. Geotech. J.* 27 (1), 151–158.
- Robertson, P.K., 2009. Interpretation of cone penetration tests—a unified approach. *Can. Geotech. J.* 46 (11), 1337–1355.
- Rodger, A., Littlejohn, G., 1980. A study of vibratory driving in granular soils. *Géotechnique* 30 (3), 269–293.
- Skau, K.S., Page, A.M., Kaynia, A.M., Løvholt, F., Norén-Cosgriff, K., Sturm, H., Andersen, H., Nygard, T., Jostad, H.P., Eiksund, G., et al., 2018. REDWIN-REDucing cost in offshore WIND by integrated structural and geotechnical design. In: *Journal of Physics: Conference Series*, Vol. 1104, No. 1. IOP Publishing, 012029.

- Spruit, R., van Tol, F., Broere, W., Slob, E., Niederleithinger, E., 2014. Detection of anomalies in diaphragm walls with crosshole sonic logging. *Can. Geotech. J.* 51 (4), 369–380.
- Stehly, T.J., Beiter, P.C., 2020. 2018 Cost of Wind Energy Review. Technical Report, National Renewable Energy Lab. (NREL), Golden, CO (United States).
- Tsetas, A., Gómez, S.S., Tsouvalas, A., van Beek, K., Tehrani, F.S., Kementzetzidis, E., Pisanò, F., Elkadi, A., Segeren, M., Molenkamp, T., Metrikine, A.V., 2020. Experimental identification of the dynamic behaviour of pile-soil system installed by means of three different pile-driving techniques. In: *Proceedings of the XI International Conference on Structural Dynamics, Vol. II. EUROdyn 2020*, European Association for Structural Dynamics, pp. 3005–3015.
- Tsetas, A., Tsouvalas, A., Metrikine, A.V., 2021. Installation of large-diameter monopiles: Introducing wave dispersion and non-local soil reaction. *J. Mar. Sci. Eng.* 9 (3), 313.
- Tsouvalas, A., 2020. Underwater noise emission due to offshore pile installation: A review. *Energies* 13 (12), 3037.
- Tsouvalas, A., Metrikine, A., 2013. A semi-analytical model for the prediction of underwater noise from offshore pile driving. *J. Sound Vib.* 332 (13), 3232–3257.
- Tsouvalas, A., Metrikine, A., 2016a. Noise reduction by the application of an air-bubble curtain in offshore pile driving. *J. Sound Vib.* 371, 150–170.
- Tsouvalas, A., Metrikine, A.V., 2016b. Structure-borne wave radiation by impact and vibratory piling in offshore installations: From sound prediction to auditory damage. *J. Mar. Sci. Eng.* 4 (3), 44.
- Versteijlen, W., Renting, F., Van Der Valk, P., Bongers, J., Van Dalen, K., Metrikine, A., 2017. Effective soil-stiffness validation: Shaker excitation of an in-situ monopile foundation. *Soil Dyn. Earthq. Eng.* 102, 241–262.
- Vos, P., 2015. Origin of the Dutch Coastal Landscape: Long-Term Landscape Evolution of the Netherlands During the Holocene, Described and Visualized in National, Regional and Local Palaeogeographical Map Series. *Barkhuis*.
- Whenham, V., 2011. Power transfer and vibrator-pile-soil interactions within the framework of vibratory pile driving (Ph.D. thesis. Doctoral thesis). University of Louvain, Belgium.
- Wu, X., Hu, Y., Li, Y., Yang, J., Duan, L., Wang, T., Adcock, T., Jiang, Z., Gao, Z., Lin, Z., et al., 2019. Foundations of offshore wind turbines: A review. *Renew. Sustain. Energy Rev.* 104, 379–393.